Coordination of Cu^{2+} Ions to C_2 Symmetric Pseudopeptides Derived from Valine

Salvador Blasco,[‡] M. Isabel Burguete,[†] M. Paz Clares,[‡] Enrique García-España,*[‡] Jorge Escorihuela,[†] and Santiago V. Luis*[†]

[†]*Departamento de Química Inorgánica y Orgánica, Universitat Jaume I, Avda. Sos Baynat s/n., 12071 Castellón, Spain, and* [‡]*Instituto de Ciencia Molecular (ICMOL), Departamento de Química Inorgánica, Universidad de Valencia, C/Catedrático José Beltrán 2, 46980 Paterna (Valencia), Spain*

The acid–base and coordination properties of a family of pseudopeptidic ligands with C_2 symmetry derived from valine (**4a**–**e**) have been studied using a variety of techniques as a model for metal coordination in peptides and proteins. The Cu^{2+} cation has been selected for coordination studies, although, for comparison, some results for Zn^{2+} are also presented. Good agreement has been obtained between the results obtained by potentiometric titrations, spectroscopic analysis, and mass spectrometry (ESI) studies. These results highlight the potential for the use of ESI MS for characterizing the nature of the complex species formed. Clearly, the Cu^{2+} complexes are much more stable than the Zn^{2+} complexes. While the role of the aliphatic spacer seems to be very minor in the case of the Zn^{2+} complexes, revealing the ability of this cation to accommodate different coordination environments, this role is critical in the case of Cu^{2+}. Different complexes with 1:1 or 2:2 Cu^{2+}:**L** stoichiometries can be formed according to the length of the spacer and the basicity of the media. This is fully illustrated by the resolution of the X-ray structures of two different Cu^{2+} complexes corresponding to the ligands containing a spacer with two methylene groups (ligand **4a**, complex **6a** [Cu$_2$(H$_{-1}$**L**)$_2$](ClO$_4$)$_2$ with a 2:2 stoichiometry) and a propylene spacer (**4b**, complex **5b** [CuH$_{-2}$**L**]·CH$_3$CH$_2$OH with a 1:1 stoichiometry).

Introduction

Coordination chemistry in metalloproteins is dominated by amino acids since amino acid side chains and backbone heteroatoms entail the majority of ligands available to coordinate to metal ions.[1] The design of new small-molecule ligands to model such challenging structural and/or functional motifs is essential for new developments in bioinorganic chemistry.[2] Although many model complexes use non-amino acid ligands that mimic various aspects of the ligand environment found in the protein, there is no doubt that the development of new ligands based on the presence of amino acid subunits is a fundamental approach in this area.[3,4]

Thus, a large number of pseudopeptidic structures have been designed in recent years for multiple purposes, and we have been involved in the preparation and study of a broad family of pseudopeptides with C_2 symmetry. Open-chain pseudopeptides such as **4** have been used as building blocks for the construction of macrocyclic structures. The corresponding macrocyclization processes have been based on the preorganization induced by conformational elements[5] or configurational factors[6] or through the use of anionic templates.[7] Some of those systems are able to display interesting features such as their behavior as organogelators,[8] acting as "in vivo" fluorescent pH probes,[9] as selective receptors for substrates of

*To whom correspondence should be addressed. E-mail: luiss@qio.uji.es (S.V.L.), enrique.garcia-es@uv.es (E.G.-E.).

(1) Roat-Malone, R. M. *Bioinorganic Chemistry: A Short Course*, 2nd ed.; John Wiley & Sons, Inc.: Hoboken, NJ, 2007.

(2) Karlin, K. D. *Science* **1993**, *261*, 701–708.

(3) (a) Sigel, H.; Martin, R. B. *Chem. Rev.* **1982**, *82*, 385–426. (b) Lucet, D.; Le Gall, T.; Mioskowski, C. *Angew. Chem., Int. Ed.* **1998**, *37*, 2580–2627. (c) Fache, F.; Schulz, E.; Tommasino, M. L.; Lemaire, M. *Chem. Rev.* **2000**, *100*, 2159–2231. (d) Hechavarría-Fonseca, M.; König, B. *Adv. Synth. Catal.* **2003**, *345*, 1173–1185. (e) Kizirian, J.-C. *Chem. Rev.* **2008**, *108*, 140–205. (f) Prell, J. S.; Flick, T. G.; Oomens, J.; Berden, G.; Williams, E. R. *J. Phys. Chem. A* **2010**, *114*, 854–860.

(4) (a) Burke, S. K.; Xu, Y.; Margerum, D. W. *Inorg. Chem.* **2003**, *42*, 5807–5817. (b) Green, B. J.; Tesfai, T. M.; Margerum, D. W. *Inorg. Chem.* **2004**, *43*, 1463–1471. (c) Green, B. J.; Tesfai, T. M.; Margerum, D. W. *Dalton Trans.* **2004**, 3508–3514. (d) Tesfai, T. M.; Green, B. J.; Margerum, D. W. *Inorg. Chem.* **2004**, *43*, 6726–6733.

(5) (a) Adrián, F.; Burguete, M. I.; Luis, S. V.; Miravet, J. F.; Querol, M.; García-España, E. *Tetrahedron Lett.* **1999**, *40*, 1039–1040. (b) Becerril, J.; Bolte, M.; Burguete, M. I.; Galindo, F.; García-España, E.; Luis, S. V.; Miravet, J. F. *J. Am. Chem. Soc.* **2003**, *125*, 6677–6686.

(6) (a) Bru, M.; Alfonso, I.; Burguete, M. I.; Luis, S. V. *Tetrahedron Lett.* **2005**, *46*, 7781–7785. (b) Alfonso, I.; Bolte, M.; Bru, M.; Burguete, M. I.; Luis, S. V. *Chem.—Eur. J.* **2008**, *14*, 8879–8891.

(7) (a) Bru, M.; Alfonso, I.; Burguete, M. I.; Luis, S. V. *Angew. Chem., Int. Ed.* **2006**, *45*, 6155–6159. (b) Alfonso, I.; Bolte, M.; Bru, M.; Burguete, M. I.; Luis, S. V.; Rubio, J. *J. Am. Chem. Soc.* **2008**, *130*, 6137–6144.

(8) (a) Becerril, J.; Escuder, B.; Miravet, J. F.; Gavara, R.; Luis, S. V. *Eur. J. Org. Chem.* **2005**, 481–485. (b) Becerril, J.; Burguete, M. I.; Escuder, B.; Luis, S. V.; Miravet, J. F.; Querol, M. *Chem. Commun.* **2002**, 738–739. (c) Becerril, J.; Burguete, M. I.; Escuder, B.; Galindo, F.; Gavara, R.; Miravet, J. F.; Luis, S. V.; Peris, G. *Chem.—Eur. J.* **2004**, 3879–3890. (d) Burguete, M. I.; Galindo, F.; Gavara, R.; Izquierdo, M. A.; Lima, J. C.; Luis, S. V.; Parola, A. J.; Pina, F. *Langmuir* **2008**, *24*, 9795–9803. (e) Burguete, M. I.; Izquierdo, M. A.; Galindo, F.; Luis, S. V. *Chem. Phys. Lett.* **2008**, *460*, 503–506.

(9) Galindo, F.; Burguete, M. I.; Vigara, L.; Luis, S. V.; Kabir, N.; Gavrilovic, J.; Russell, D. A. *Angew. Chem., Int. Ed.* **2005**, *44*, 6504–6508.

Scheme 1. Synthesis of Chiral Bis(Amino Amide) Ligands Derived from Valine[a]

3a–e; n = 0, 1, 2, 3, 4   **4a–e; n = 0, 1, 2, 3, 4**
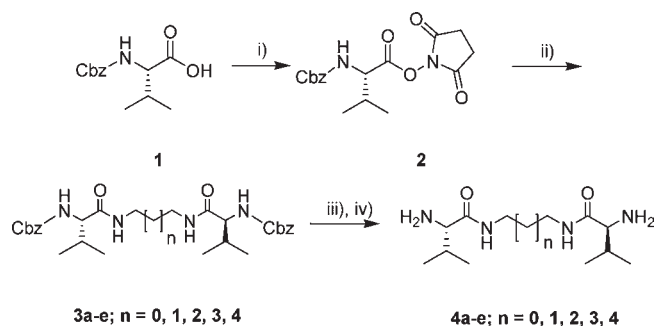
[a] Reagents: (i) DCC, N-hydroxysuccinimide, THF, rt. (ii) H_2NCH_2-$(CH_2)_nCH_2NH_2$, DME, rt. (iii) HBr/AcOH. (iv) $NaOH_{aq}$.

Table 1. Stepwise and Cumulative Basicity Constants of Compounds **4a–e** Determined in 0.15 M $NaClO_4$ at 298.1 K

reaction[a]	4a	4b[b]	4c	4d	4e
$H + L \rightleftharpoons HL$	7.94(1)[c]	8.008(5)	8.126(3)	8.111(4)	8.16(1)
$H + HL \rightleftharpoons H_2L$	6.96(1)	6.956(7)	7.319(4)	7.312(4)	7.367(1)

[a] Charges omitted. [b] Determined in 0.15 M NaCl. [c] Values in parentheses are standard deviations in the last significant figure.

Figure 1. Distribution diagram for the protonated species of **4a** in 0.15 M $NaClO_4$ at 298.1 K.

biological relevance,[10] as minimalistic molecular machines,[11] or as ligands for the preparation of enantioselective catalysts, of particular efficiency in the case of the enantioselective addition of dialkylzinc to aromatic aldehydes.[12] On the other hand, the self-assembly of this kind of compound in the solid state has also given rise to the observation of some remarkable crystalline structures and nanoassembled morphologies with relevance for the understanding of structural parameters in proteins and related systems.[13]

Here, we present the study of the acid−base properties of some valine-derived open-chain pseudopeptides of this class (**4a–e**), as well as the analysis of their binding ability toward a cation playing a key role in bioinorganic chemistry such as Cu^{2+}. Some data for Zn^{2+} are also presented. Interesting variations in the complexes formed are observed as a consequence of the modification of the aliphatic spacer. The structure of some of those complexes has been determined by X-ray crystallography. The combination of a set of different complementary techniques including pH-metric titrations, ESI-MS, UV−vis spectroscopy, and X-ray diffraction analysis has allowed the achievement of an in depth knowledge of these systems.

Results and Discussion

Equilibrium Studies on Ligand Protonation and on the Formation of Cu^{2+} and Zn^{2+} Complexes. EMF Measurements. The synthesis of the receptors was carried out following previously reported procedures, as is outlined in Scheme 1.[5]

Acid−Base Behavior. The study of the acid−base properties of the receptors is essential for a proper understanding of the coordination properties of nitrogenated compounds.[14,15]

Acid−base properties of compounds **4** were studied by the use of pH-metric titrations. All the titrations were carried out as has been fully described,[16] at 298.1 K using 0.15 M $NaClO_4$ to maintain a constant ionic strength. The program PASAT was used for data acquisition.[17] The program HYPERQUAD[18] was employed for calculating the stability constants, and the program HYSS was used to obtain the distribution diagrams.[19] The stepwise and cumulative stability constants for the protonation of receptors **4**, obtained in this way, are presented in Table 1.

All the compounds show two stepwise basicity constants within the pH range of the study (2−11) that correspond to the protonation processes of the primary amino groups. Although there is a very slight increase in basicity following the increase in the number of methylene groups in the bridge separating the amide groups, the most noticeable aspect is, however, the resemblance of the stepwise basicity constants for all these compounds. The separation between positive charges is high enough to make the basicity of all these compounds very close between them.[20] Accordingly, very similar distribution diagrams for the protonated species were obtained for all receptors **4**. As an example, the distribution diagram for the smaller compound, **4a**, is presented in Figure 1. The distribution diagrams for all protonations are collected in Figure S2 of the Supporting Information.

(10) (a) Burguete, M. I.; Galindo, F.; Izquierdo, M. A.; Luis, S. V.; Vigara, L. *Tetrahedron* **2007**, *63*, 9493–9500. (b) Alfonso, I.; Burguete, M. I.; Galindo, F.; Luis, S. V.; Vigara, L. *J. Org. Chem.* **2009**, *74*, 6130–6142. (c) Burguete, M. I.; Galindo, F.; Luis, S. V.; Vigara, L. *J. Photochem. Photobiol. A* **2010**, *209*, 61–67.

(11) (a) Alfonso, I.; Burguete, M. I.; Luis, S. V. *J. Org. Chem.* **2006**, *71*, 2242–2250. (b) Alfonso, I.; Burguete, M. I.; Galindo, F.; Luis, S. V.; Vigara, L. *J. Org. Chem.* **2007**, *72*, 7947–7956.

(12) (a) Adrián, F.; Burguete, M. I.; Fraile, J. M.; García, J. I.; García-España, E.; Luis, S. V.; Mayoral, J. A.; Royo, A. J.; Sánchez, M. C. *Eur. J. Inorg. Chem.* **1999**, 2347–2354. (b) Burguete, M. I.; Escorihuela, J.; Luis, S. V.; Lledós, A.; Ujaque, G. *Tetrahedron* **2008**, *64*, 9717–9724.

(13) (a) Alfonso, I.; Bolte, M.; Bru, M.; Burguete, M. I.; Luis, S. V. *CrystEngComm* **2009**, *11*, 735–738. (b) Alfonso, I.; Bru, M.; Burguete, M. I.; García-Verdugo, E.; Luis, S. V. *Chem.—Eur. J.* **2010**, *16*, 1246–1255. (c) Becerril, J.; Bolte, M.; Burguete, M. I.; Escorihuela, J.; Galindo, F.; Luis, S. V. *CrystEngComm* **2010**, *12*, 1722–1725.
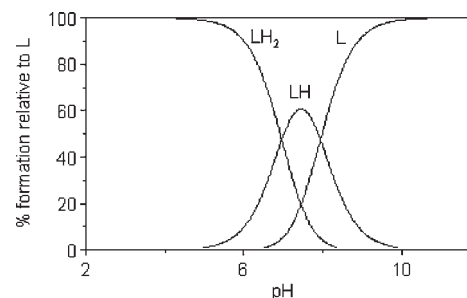
(14) García-España, E.; Díaz, P.; Llinares, J. M.; Bianchi, A. *Coord. Chem. Rev.* **2006**, *250*, 2952–2986.

(15) Martell, A. E.; Motekaitis, R. J. *Coord. Chem. Rev.* **1990**, *100*, 323–361.

(16) (a) García-España, E.; Ballester, M.-J.; Lloret, F.; Moratal, J. M.; Faus, J.; Bianchi, A. *J. Chem. Soc., Dalton Trans.* **1988**, 101–104. (b) Burguete, M. I.; García-España, E.; López-Diago, L.; Luis, S. V.; Miravet, J. F.; Sroczynski, D. *Org. Biomol. Chem.* **2007**, *5*, 1935–1944.

(17) Fontanelli, M.; Micheloni, M. Program for the automatic control of the microburette and the acquisition of the electromotive force readings. *Proceedings of the I Spanish-Italian Congress on Thermodinamics of Metal Complexes*, Peñíscola, Castellón, Spain, 1990.

(18) Gans, P.; Sabatini, A.; Vacca, A. *Talanta* **1996**, *43*, 1739–1753.

(19) Alderighi, L.; Gans, P.; Ienco, A.; Peters, D.; Sabatini, A.; Vacca, A. *Coord. Chem. Rev.* **1999**, *184*, 311–318.

(20) (a) Sarnesky, J. E.; Surprenant, H. L.; Molen, F. K.; Reiley, C. N. *Anal. Chem.* **1975**, *47*, 2116–2124. (b) Frassineti, C.; Ghelli, S.; Gans, P.; Sabatini, A.; Moruzzi, M. S.; Vacca, A. *Anal. Biochem.* **1995**, *231*, 374–382. (c) Frassineti, C.; Alderighi, L.; Gans, P.; Sabatini, A.; Vacca, A. *Anal. Bioanal. Chem.* **2003**, *376*, 1041–1052.

Chart 1. Proton Assignment for NMR Studies
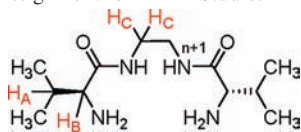
Table 2. Protonation Induced Observed Shifts in the δ Values for the Different Hydrogen Atoms of **4a** in D_2O at 303 K, Working at 500 MHz

pD	$\Delta\delta\ H_A$	$\Delta\delta\ H_B$	$\Delta\delta\ H_c$
12.67			
9.96	0.00	0.00	0.00
8.55	0.07	0.13	0.00
7.63	0.15	0.41	0.02
6.53	0.30	0.62	0.03
4.86	0.37	0.73	0.10
2.82	0.33	0.68	0.04

The protonation process can also be monitored through the use of ^{1}H NMR spectroscopy. NMR spectroscopy can give interesting information regarding protonation sequences, in particular, when the nitrogen atoms bearing the protons present different chemical environments.[21] It is well established that upon protonation of polyamine compounds, the hydrogen nuclei attached to the carbon in the α position to the nitrogen atom bearing the proton are those exhibiting the largest downfield changes in their chemical shift.[22] Therefore, to obtain further information about the protonation sequence of the compounds, the ^{1}H NMR spectra of the ligands versus pD were recorded. For all the cases, the protonation of the amino groups is accompanied, as could be expected, by a significant downfield shift of the proton H_b (see Chart 1) attached to the stereogenic carbon atom and also by a smaller downfield shift of the proton H_a of the isopropyl group. The protonation also has a minor effect on the shift of protons H_c located at the spacer.

As an example, the $\Delta\delta$ values obtained for **4a** at different pD values, taking the spectrum at pH 12.7 as the reference, are given in Table 2. It is worth mentioning that for the three studied protons (for signals of protons H_A, H_B, and H_C), the δ values steadily increase on going from basic to acidic regions, reaching a maximum around pD = 5 in correspondence with the completion of the second protonation. At more acidic pH regions, a slight decrease in the corresponding $\Delta\delta$ values is observed. This suggests that in order to minimize electrostatic repulsions, a significant conformational change takes places when

Figure 2. Minimum energy conformers calculated for nonprotonated (**L**), monoprotonated (**HL**), and diprotonated (**H_2L**) **4a**.

both amino groups are protonated, most likely to achieve an extended conformation in order to minimize electrostatic repulsions.

In this regard, molecular modeling calculations to get further information and better analyze this process were also performed.[23] The structures of the local minima obtained for each protonated state were in good agreement with the process suggested by NMR data. To obtain the corresponding energy minima by molecular modeling, the conformer distribution calculation option available in Spartan 04 was used.[24] With this option, an exhaustive Monte Carlo search without constraints was performed for every structure. The torsion angles were randomly varied and the obtained structures fully optimized using the MMFF force field. Thus, 100 minima of energy within an energy gap of 10 kcal/mol were generated for each protonated state of the different receptors. These structures were analyzed and ordered considering their relative energy, the repeated geometries being eliminated. Similar results were obtained for all the ligands. Although a significant number of different conformations are obtained within the considered energy gap, all of them maintain some common structural elements and confirm the predominance of very different conformations for monoprotonated (**HL**) and diprotonated (**H_2L**) species. This can be observed for the minimum energy conformers of **4a** depicted in Figure 2. Both the nonprotonated (**L**) and the monoprotonated (**HL**) species present folded conformations, while the diprotonated (**H_2L**) species presents an extended conformation in order to minimize electrostatic repulsions. The folded arrangement for the nonprotonated and monoprotonated system favors their stabilization through intramolecular H-bonding and additional electrostatic interactions.

Determination of the Cu^{2+} Complexes Formation Constants. Because of the interest in developing copper-containing model systems for metalloproteins,[25] and taking into account our previous experience in this field, for instance in the study of simplified HCA models,[26] the synthesis and study of copper and zinc complexes of those compounds was carried out. In this regard, Cu^{2+} complexes could be easily obtained by the reaction of one equivalent of the bis(amino amide) ligands **4** and one equivalent of Cu^{2+} acetate in basic

(21) (a) Dagnall, S. P.; Hague, D. N.; McAdam, M. E. *J. Chem. Soc., Perkin Trans. 2* **1984**, 1111–1114. (b) Hague, D. N.; Moreton, A. D. *J. Chem. Soc., Perkin Trans. 2* **1994**, 265–270. (c) Bianchi, A.; Escuder, B.; García-España, E.; Luis, S. V.; Marcelino, V.; Miravet, J. F.; Ramírez, J. A. *J. Chem. Soc., Perkin Trans. 2* **1994**, 1253–1259. (d) Aguilar, A.; García-España, E.; Luis, S. V.; Llinares, J. M.; Miravet, J. F.; Ramírez, J. A.; Soriano, C. *Inorg. Chim. Acta* **1996**, *246*, 287–294. (e) Aran, V. J.; Kumar, M. J.; Molina, J.; Lamarque, L.; Navarro, P.; García-España, E.; Ramirez, J. A.; Luis, S. V.; Escuder, B. *J. Org. Chem.* **1999**, *64*, 6135–6146.

(22) (a) Dagnall, S. P.; Hague, D. N.; McAdam, M. E. *J. Chem. Soc., Perkin Trans. 2* **1984**, 435–440. (b) Alderighi, L.; Bianchi, A.; Biondi, L.; Calabi, L; De Miranda, M.; Gans, P.; Ghelli, S.; Losi, P.; Paleari, L.; Sabatini, A.; Vacca, A. *J. Chem. Soc., Perkin Trans. 2* **1999**, 2741–2745. (c) Bencini, A.; Bianchi, A.; García-España, E.; Micheloni, M.; Ramírez, J. A. *Coord. Chem. Rev.* **1999**, *188*, 97–156. (d) Aguilar, J.; Díaz, P.; Escartí, F.; García-España, E.; Gil, L.; Soriano, C.; Verdejo, B. *Inorg. Chim. Acta* **2002**, *39*, 307–316. (e) Albelda, M. T.; Frias, J. C.; García-España, E. *Encycl. Supramol. Chem.* **2007**, *1:1*, 1.

(23) (a) Burguete, M. I.; Escuder, B.; García-España, E.; Luis, S. V.; Miravet, J. F. *J. Org. Chem.* **1994**, *59*, 1067–1071. (b) Altava, B.; Bianchi, A.; Bazzicalupi, C.; Burguete, M. I.; García-España, E.; Luis, S. V.; Miravet, J. F. *Supramol. Chem.* **1997**, *8*, 287–299. (c) Albelda, M. T.; Frías, J. C.; García-España, E.; Luis, S. V. *Org. Biomol. Chem.* **2004**, *2*, 816–820.

(24) *Spartan 04*; Wavefunction, Inc.: Irvine, CA. For MMFF force field calculations, see: Halgren, T. A. *J. Comput. Chem.* **1996**, *17*, 490−519 and following papers in this issue.

(25) Stephens, J. C.; Khan, M. A.; Houser, R. P. *Inorg. Chem.* **2001**, *40*, 5064–5065.

(26) (a) Altava, B.; Burguete, M. I.; Luis, S. V.; Miravet, J. F.; García-España, E.; Marcelino, V.; Soriano, C. *Tetrahedron* **1997**, *53*, 4751–4762. (b) Andrés, S.; Escuder, B.; Doménech, A.; García-España, E.; Luis, S. V.; Marcelino, V.; Llinares, J. M.; Ramírez, J. A.; Soriano, C. *J. Phys. Org. Chem.* **2001**, *14*, 495–500.

Table 3. Logarithms of the Formation Constants for the Cu^{2+} Complexes of Ligands **4a−e** Determined in 0.15 M $NaClO_4$ at 298.1 K

reaction[a]	4a	4b[b]	4c	4d	4e
$Cu + L \rightleftharpoons CuL$	6.09(4)[c]	5.99(3)	7.03(1)	6.76(1)	7.14(2)
$Cu + L + H \rightleftharpoons CuHL$			12.64(2)	12.51(4)	12.67(6)
$Cu + L \rightleftharpoons CuH_{-1}L + H$	0.67(1)	0.53(1)	−0.04(2)	−0.23(2)	−0.04(2)
$Cu + L \rightleftharpoons CuH_{-2}L + 2H$	−6.48(1)	−6.66(1)	−6.61(1)	−9.89(3)	−9.78(3)
$CuL + H \rightleftharpoons CuHL$			5.61(2)	5.74(3)	5.53(5)
$CuL \rightleftharpoons CuH_{-1}L + H$	−5.42(4)	−5.46(3)	−7.07(1)	−7.00(2)	−7.19(2)
$CuH_{-1}L \rightleftharpoons CuH_{-2}L + H$	−7.15(2)	−7.19(1)	−6.56(2)	−9.66(4)	−9.74(3)

[a] Charges omitted for clarity. [b] Determined in 0.15 M NaCl. [c] Values in parentheses are standard deviations in the last significant figure.
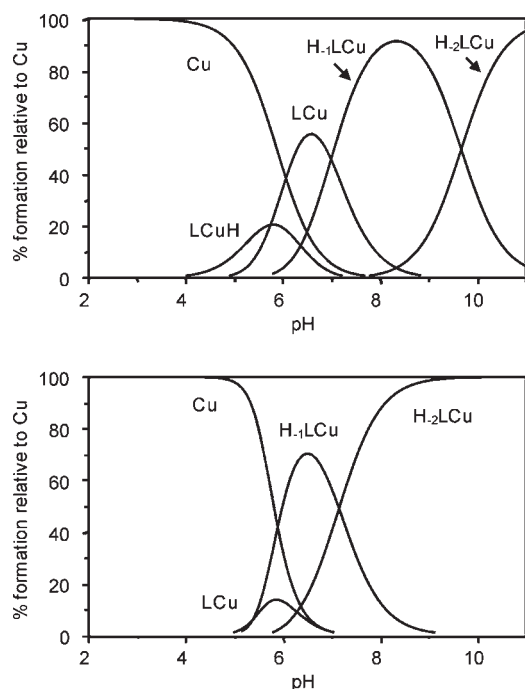
Figure 3. Distribution diagrams for the systems Cu^{2+}−**4a** (bottom) and Cu^{2+}−**4d** (top) determined in 0.15 M $NaClO_4$.

methanol to afford bright-colored solids. The interaction of Cu^{2+} and ligands **4** was systematically studied by potentiometric titrations in aqueous solution over the 2−11 pH range. The stability constants for the formation of Cu^{2+} complexes have been determined in water using 0.15 M $NaClO_4$ to maintain a constant ionic strength and a temperature of 298.1 K. The results obtained are presented in Table 3.

All the compounds in this series show a similar speciation with the formation of a nondeprotonated $[CuL]^{2+}$ species and two deprotonated species $[CuH_{-1}L]^+$ and $[CuH_{-2}L]$. Apart from these species, a monoprotonated $[CuHL]^{3+}$ species has also been detected for the compounds with longer hydrocarbon chains between the coordination sites (**4c−e**). According to the general structure of compounds **4**, it seems reasonable to assume that the formation of monocationic $[CuH_{-1}L]^+$ and neutral $[CuH_{-2}L]$ species takes place through deprotonation of the N−H amide functional groups. This was further inferred from their infrared and visible electronic spectra and supported by the two crystal structures solved by X-ray diffraction (see below). The values of the constants in Table 3 and the distribution diagrams (Figure 3, bottom) show that the three shortest ligands, **4a**, **4b**, and **4c**, undergo deprotonation of the amido groups at relatively low pH values. Moreover, for **4c**, both deprotonations proceed in a cooperative way, so that a pH range where

the monodeprotonated species predominates in solution cannot be distinguished. For the largest two ligands (**4d** and **4e**), there is a greater separation between the deprotonation of the first and second amide groups that occurs at more basic pH values (Figure 3, top). See the Supporting Information for the distribution diagrams for **4b**, **4c**, and **4e**.

Coordination of Cu^{2+} to the shortest ligands induces a drop in basicity of the amide groups of over 5 orders of magnitude. As a matter of fact, the nondeprotonated $[CuL]^{2+}$ species do not predominate at any pH value, being only major species in solution complexes with deprotonated amide groups. At this point, some concern can exist with regard to the structure of the $[CuH_{-1}L]^+$ species for **4a**, since in the solid state it presented a polymeric structure.

The behavior of the two largest ligands is represented by the distribution diagram shown at the top of Figure 3. In this case, the $[CuL]^{2+}$ species prevails in a narrow 6−7 pH window, and although the inductive effects generated by the metal are still very important, the amide groups, particularly the second one, deprotonate at higher pH values.

Determination of the Zn^{2+} Complexes' Formation Constants. For the sake of comparison, a similar study to that reported above for Cu^{2+} was carried out for the determination of the Zn^{2+} complexes' formation constants. The stability constants for the formation of Zn^{2+} complexes were determined by potentiometic titrations in water using 0.15 M $NaClO_4$ to maintain constant the ionic strength and a temperature of 298.1 K and are presented in Table 4.

Significant differences can be observed when the data in Table 4 are compared with those obtained for Cu^{2+} complexes. The most remarkable observation is the low stability of the Zn^{2+} complexes formed. Although lower values of the stability constants are expected when the Zn^{2+} complexes are compared with those of Cu^{2+} for a given ligand, the values obtained are even some orders of magnitude lower than those reported for the Zn^{2+} complexes of other tetradentated ligands.[27] As a matter of fact, only the formation of $[ZnH_{-2}L]$ complex species is observed above pH 8. As in the case of Cu^{2+} complexes, ligands **4** can be grouped in two categories. For receptors **4a,b** containing the shortest spacers (see the Supporting Information for the corresponding distribution diagrams), only the $[ZnH_{-2}L]$ species are essentially detected above pH 8; a minor contribution of $[ZnL]$ is also observed for **4a** (**L1**). For the ligands **4c−e** (**L3−L5**) containing longer spacers, some additional complex species are detected at the 5−9 pH window, although, in all cases, those species are always very minor. The fact that the length

(27) (a) Lamarque, L.; Navarro, P.; Miranda, C.; Arán, V. J.; Ochoa, C.; Escartí, F.; García-España, E.; Latorre, J.; Luis, S. V.; Miravet, J. F. *J. Am. Chem. Soc.* **2001**, *123*, 10560–10570. (b) Burguete, M. I.; Escuder, B.; García-España, E.; Luis, S. V.; Miravet, J. F. *Tetrahedron* **2002**, *58*, 2839–2846.

Table 4. Logarithms of the Formation Constants for the Zn^{2+} Complexes of Receptors **4a–e** Determined in 0.15 M $NaClO_4$ at 298.1 K

reaction[a]	4a	4b[b]	4c	4d	4e
$Zn + L \rightleftharpoons ZnL$			3.09(6)[c]	3.50(3)	3.99(2)
$Zn + L + H \rightleftharpoons ZnHL$			11.08(3)	10.86(3)	11.32(5)
$Zn + L \rightleftharpoons ZnH_{-1}L + H$			−4.9(1)	−5.1(1)	−4.53(8)
$Zn + L \rightleftharpoons ZnH_{-2}L + 2H$	−12.44(1)	−12.64(1)	−12.14(1)	−12.22(1)	−12.08(1)
$ZnL + H \rightleftharpoons ZnHL$			7.99(4)	7.36(3)	7.32(4)
$ZnL \rightleftharpoons ZnH_{-1}L + H$			−8.1(1)	−8.63(9)	−8.52(7)
$ZnH_{-1}L \rightleftharpoons ZnH_{-2}L + H$			−7.2(1)	−7.1(1)	−7.55(8)

[a] Charges omitted for clarity. [b] Determined in 0.15 M NaCl. [c] Values in parentheses are standard deviations in the last significant figure.
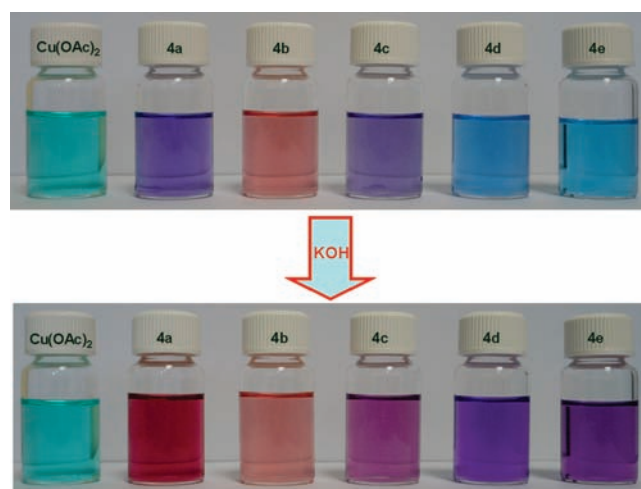
Scheme 2. Synthesis of Cu^{2+} Complexes Derived from Ligands **4**

4a-e; n = 0, 1, 2, 3, 4   **5a-e; n = 0, 1, 2, 3, 4**   **6a-e; n = 0, 1, 2, 3, 4**
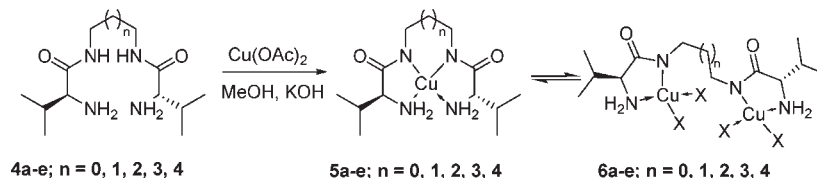
of the spacer seems to affect only to a minor extent the formation of the corresponding Zn^{2+} complexes is in good agreement with the results reported for those ligands as catalysts for the Et_2Zn addition to aldehydes.[12b] In this case, it has been shown that catalytic results are essentially independent of the spacer. Those results suggest that Zn^{2+} is able to easily accommodate the changes forced in its coordination sphere by the modification of the spacer. Nevertheless, this must be taken with caution, as the catalytic experiments have been carried out in hexanes and other organic solvents

Spectroscopic and Spectrometric Studies on the Formation of Cu^{2+} and Zn^{2+} Complexes.   Spectroscopic Studies. In order to gain more detailed insight into the nature of the complex species formed by receptors **4** (**L**) and Cu^{2+} and Zn^{2+}, a spectroscopic study was carried out, taking advantage of the data provided by the distribution diagrams formerly obtained. In the case of Cu^{2+}, both UV–visible and IR spectroscopies were used; while in the case of Zn^{2+}, only IR spectroscopy could be applied. In both cases, this study was completed by the use of mass spectrometry (ESI-MS), as will be discussed below.

As mentioned before, Cu^{2+} complexes can be obtained by reaction of one equivalent of **4** and one equivalent of Cu^{2+} acetate in basic methanol (KOH). The structures postulated in Scheme 2 are presented according to experimental evidence. Upon complexation, the carbonyl frequency (FT-IR) shifts from 1663 cm^{-1} in compounds **4** to 1566 cm^{-1} in complexes **5**, indicating the participation of the deprotonated amide group in the coordination to Cu^{2+} in agreement with the data obtained by potentiometry and with related systems.[28] The same shifts in the carbonyl band are also observed for the formation of Zn^{2+} complexes, although in this case colorless complexes are obtained.

Besides the chelate complexes **5** ($CuH_{-2}L$), other structures like the ones represented in **6** ($Cu_2(H_{-2}L)X_4$) can also be considered. In this case, a variety of ligands can stand for X, including donor atoms (N, O) from other

(28) (a) Wagler, T. R.; Fang, Y.; Burrows, C. J. *J. Org. Chem.* **1989,** *54,* 1584–1589. (b) Dangel, B.; Clarke, M.; Haley, J.; Sames, D; Polt, R. *J. Am. Chem. Soc.* **1997,** *119,* 10865–10866. (c) Weeks, C. L.; Turner, P.; Fenton, R. R.; Lay, P. A. *J. Chem. Soc., Dalton Trans.* **2002,** 931–940. (d) Burguete, M. I.; Galindo, F.; Luis, S. V.; Vigara, L. *Dalton Trans.* **2007,** 4027–4033. (e) Shakya, R.; Jozwiuk, A.; Powell, D. R.; Houser, R. P. *Inorg. Chem.* **2009,** *48,* 4083–4088.
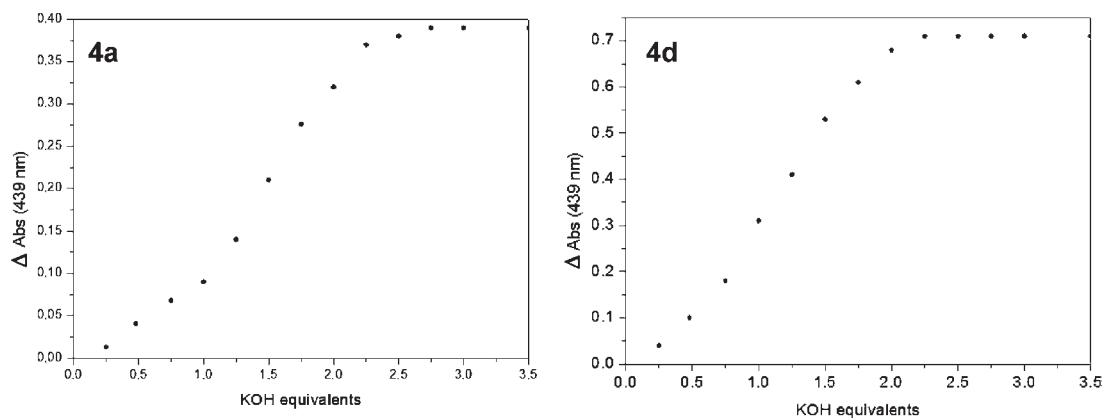
Figure 4. Complex formation in MeOH from receptors **4** and $Cu(OAc)_2$ under neutral conditions (top) and after the addition of two equivalents of KOH (bottom).

pseudopeptidic structures. The complexes formed by Cu^{2+} in methanolic solution under neutral conditions show, in all cases, a blue coloration that sharply changes when a base is added to afford solutions with colors ranging from red-orange to violet depending on the ligand used, as shown in Figure 4. The most significant spectroscopic data for those complexes obtained under basic conditions are gathered in Table 5. The preferential formation, under basic conditions, of $[CuH_{-2}L]$ complex species derived from the double deprotonation of the ligand at both amide groups, was confirmed by UV–visible titrations. For this purpose, the reactants, the corresponding receptor **4** and Cu^{2+} acetate, were mixed (0.6 mM and 0.6 mM, respectively, in MeOH) in a spectrophotometric cell. Aliquots of a base (KOH in MeOH) were added stepwise. For the formation of metallic complexes **5** (or **6**), deprotonation of the amide group of ligands **4** is needed. Since there are two amide groups in **4**, then two equivalents of the base, relative to Cu^{2+}, would be required to form the final complex. As shown in Figure 5, the reaction of one equivalent of **4** with one equivalent of Cu^{2+} is complete after the addition of exactly two equivalents of KOH, according to UV–vis spectroscopy data.

Figure 5. Change of the absorbance (439 nm) in MeOH of a mixture of **4a** (left) or **4d** (right) (0.6 mM) and Cu(OAc)$_2$ (0.6 mM) upon the addition of KOH.
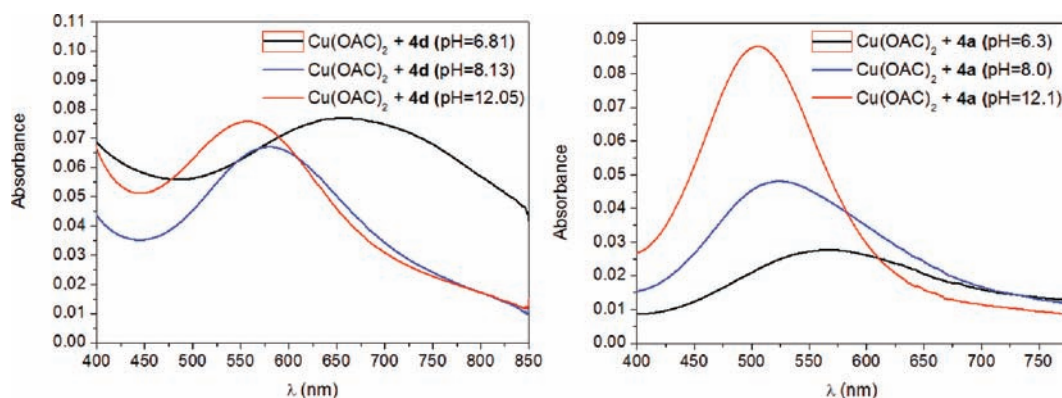

Figure 6. UV−vis spectra in water for the Cu^{2+}−**4a** and Cu^{2+}−**4d** systems at different pH values (see insets) in the 400−800 nm region.

Table 5. Spectroscopic Data for the Cu^{2+}−**4** Complexes Obtained in Methanol under Basic Conditions

compound	λ_{max} (nm)	ε (M^{-1} cm^{-1})	λ_{max} (nm)^a	$v_{(C=O)}$ (cm^{-1})
5a	439	60	502	1566
5b	437	132	496	1567
5c	455	75	510	1567
5d	440	75	553	1566
5e	445	75	518	1566

^{a} Determined in water.

The spectroscopic properties of the Cu^{2+} complexes formed do not differ greatly from methanol to water. On the other hand, the corresponding distribution diagrams provide a very useful tool to rationalize the changes observed with the pH of the medium. In the UV−vis spectra, all complexes exhibit intense ligand to metal charge transfer transitions (LMCT) in the range of 200−315 nm. In the regions where the uncomplexed cation or [CuL]$^{2+}$ complexes predominate, the maxima for the band corresponding to d−d transitions are in the 640−690 nm range, characteristic of octahedral Cu^{2+} complexes, while for regions where deprotonated complexes [CuH$_{-x}$L]$^{(2-x)+}$ are the major species, the maxima are bathochromically shifted to 490−560 nm, suggesting geometries ranging from square-planar to square-pyramidal.[29] This is well illustrated by the comparison of the UV−vis spectra obtained in water for the system Cu^{2+}−**4d** as

shown in Figure 6. At pH = 6.8, a region for which deprotonated [CuH$_{-x}$L]$^{(2-x)+}$ species only account for about 30% of the total copper concentration and [CuL]$^{2+}$ species are still predominant in solution (*ca.* 50%), the spectrum shows a broad band with its maximum at 668 nm. When a pH value of 8.1 is reached by adding NaOH, the band shifts to 578 nm, and this corresponds, at the distribution diagram, with the presence of [CuH$_{-1}$L]$^+$ as the major species (ca. 85%) along with [CuL]$^{2+}$ and [CuH$_{-2}$L] as minor species (below 5% each). Finally, at pH = 12, the maximum of the band is further shifted to 553 nm, corresponding to the presence of [CuH$_{-2}$L] as the only species in solution. A similar analysis can be carried out for the other ligands, and the corresponding spectra are presented in the Supporting Information. It is worth mentioning that for the receptors containing the shortest spacers, **4a**−**c**, the UV−vis spectra confirm, as observed in the distribution diagrams, that deprotonated complexes [CuH$_{-x}$L]$^{(2-x)+}$ start forming even without the addition of a base, at pH values of 6−7. For those cases (pH ≈ 6−7), broader bands are observed that can be deconvoluted into two bands: a more intense one centered about 650 nm and a minor one centered at 500 nm, which allows for a rough estimate of a participation below 10% of the total for those species.

The stoichiometry of the Cu^{2+} complexes in methanol was determined by the continuous variations method (Job plot).[30] For this purpose, different solutions of the

(29) Polt, R.; Kelly, B. D.; Dangel, B. D.; Tadikonda, U. B.; Ross, R. E.; Raitsimring, A. M.; Astashkin, A. V. *Inorg. Chem.* **2003**, *42*, 566–574. (b) Autzen, S.; Korth, H.-G.; Boese, R.; De Groot, H.; Sustmann, R. *Eur. J. Inorg. Chem.* **2003**, 1401–1410.

(30) (a) Schneider, H. J.; Yatsimirsky, A. *Principles and Methods in Supramolecular Chemistry*; Wiley: New York, 2000. (b) Job, P. *Ann. Chim.* **1928**, *9*, 113–203.
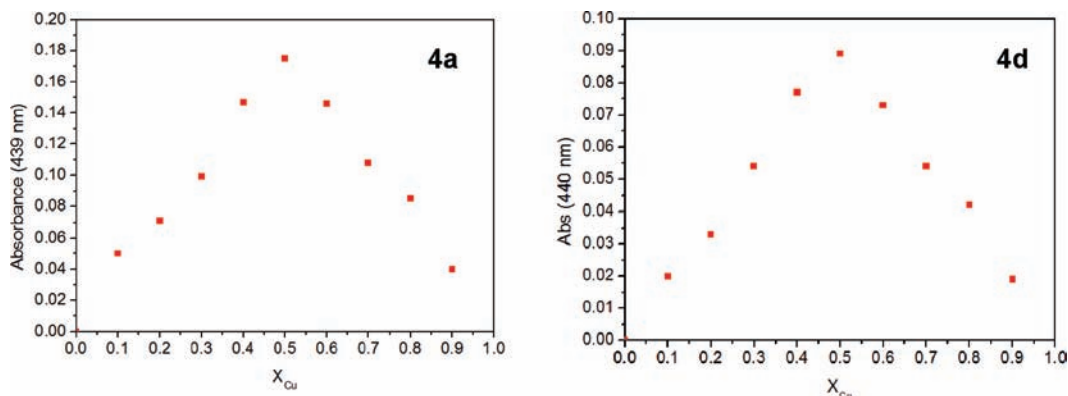
Figure 7. Job plot for ligands **4a** and **4d** and Cu(OAc)$_2$ in methanol.
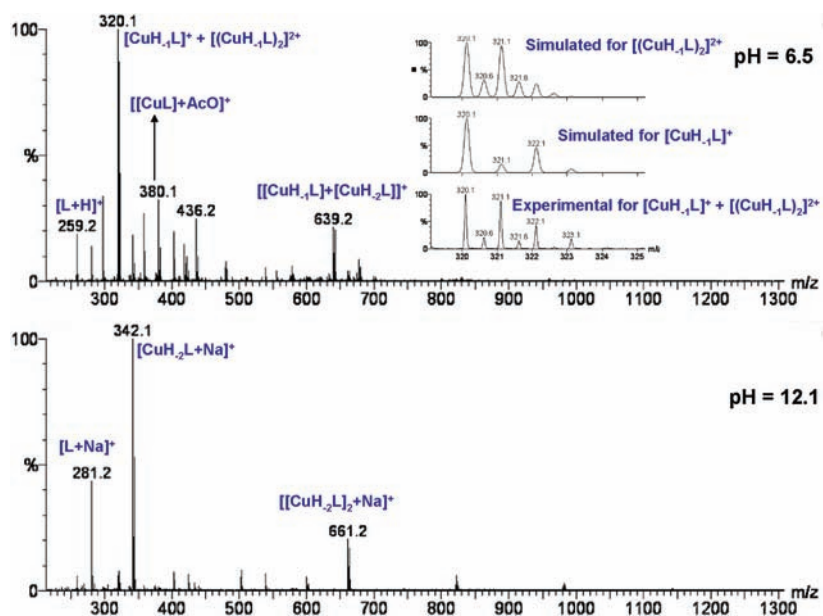

Figure 8. ESI+ MS spectra for Cu^{2+} and ligand **4a** at pH = 6.5 (top) and at pH = 12.1 (bottom) in water.

corresponding ligand containing different molar fractions of the Cu^{2+} salt were prepared with the total concentration kept constant at 3×10^{-5} M. The molar fraction of the metal salt varied in the 0.1−0.9 range. As is illustrated for **4a** and **d** in Figure 7, the Job plots showed maxima centered at a molar ratio of 0.5, indicative of a 1:1 ligand/metal stoichiometry.

Mass Spectrometry Analysis. In order to obtain additional information on the molecularity of the complexes formed, the different solutions prepared for obtaining the UV−vis spectra of Cu^{2+} species, at different pH values, were also examined by mass spectrometry.[31] In this respect, ESI-MS is a very useful technique, since it allows the detection of species at very low concentrations.[32] For this purpose, the ESI technique in the positive mode of

analysis was used. Again, similar results were obtained either in methanol or in water.[33]

For the shortest ligand **4a**, at pH values of 6.8−7.0, the observed base peak appears at 320.1 (Figure 8). This mass corresponds to the one expected for the monocationic [CuH$_{-1}$L]$^+$ species, which largely predominates in this pH region. Nevertheless, a careful analysis of the isotopic pattern of the cluster at 320.1 reveals that it is formed through the participation of the doubly charged dimer [[CuH$_{-1}$L]$_2$]$^{2+}$ along with [CuH$_{-1}$L]$^+$ (see inset of Figure 8).

The second most intense fragment (*ca.* 40%) is the one at 380.1 that can be attributed to the [[CuL]+AcO]$^+$ monocation. This corresponds with the presence at this pH of the [CuL]$^{2+}$ species as a minor component (see distribution diagram in Figure 3). A third peak of lower intensity (20%) appears at 639.2 and can be assigned to the monocationic heterodimer [[CuH$_{-1}$L][CuH$_{-2}$L]]$^+$ in accordance with the presence at this pH of ca. 25% of the fully deprotonated complex [CuH$_{-2}$L]. This is also reflected in the observation of the corresponding homodimeric species [[CuH$_{-2}$L]$_2$+Na]$^+$ at 677.2 and the peaks at 342.1 and 358.1 for [CuH$_{-2}$L]+Na]$^+$ and [CuH$_{-2}$L]+K]$^+$, respectively. It is interesting to note that those peaks are almost absent at pH = 6.9, while they reach an intensity of 20−30% at pH = 7,

(31) Gao, J.; Reibenspies, J. H.; Zingaro, R. A.; Woolley, F. R.; Martell, A. E.; Clearfield, A. *Inorg. Chem.* **2005**, *44*, 232–241.

(32) (a) Schug, K.; Fryčák, P.; Maier, N. M.; Lindner, W. *Anal. Chem.* **2005**, *77*, 3660–3670. (b) Di Tullio, A.; Reale, S.; De Angelis, F. *J. Mass Spectrom.* **2005**, *40*, 845–865. (c) Baytekin, B.; Baytekin, H. T.; Schalley, C. A. *Org. Biomol. Chem.* **2006**, *4*, 2825–2841.

(33) It is important to note that in order to optimize the ESI-MS results, some methanol was added to the purely aqueous solutions where the complexes were prepared and being used for the UV−visible analyses. No additional solvents were, however, added to the purely methanolic solutions.

in correspondence with the sharp increase in the concentration of the bis-deprotonated complex in this region. Additional fragments, corresponding either to the free ligand or to clusters derived from deprotonated complexes and including other species such as NaOAc or H_2O (i.e., 402.1 for $[[CuH_{-1}L]+NaAcO]^+$), are also detected. At a pH around 12, the situation is simpler. Here, only the $[CuH_{-2}L]$ species are present in the distribution diagram and are, essentially, the only species detected in MS. The base peak appears at 342.1, corresponding to the monocationic $[[CuH_{-2}L]+Na]^+$ species (NaOH was used as the base). In addition, a fragment at 281.2 for the free ligand $[L+Na]^+$ (ca. 45%) and a minor peak, with an intensity below 20%, at 661.2, corresponding to the monocationic homodimer $[[CuH_{-2}L]_2+Na]^+$ is also observed. Some additional fragments corresponding to other clusters can be identified, but in all cases their relative intensities fall below 10%.

The ESI^+-MS spectra obtained from methanolic solutions provide the same information, although they are slightly more complex, as under those conditions, the formation of complex aggregates is favored (see the Supporting Information).

Similar trends are observed for **4b**. At pH values of 6.5–6.6, the $[CuH_{-1}L]^+$ complex species is predominant and the corresponding base peak appears at 334.1 along with the related heterodimer $[[CuH_{-1}L][CuH_{-2}L]]^+$ at 670.3. In this case, the peak at 334.1 also contains, according to the isotopic pattern, significant amounts of the homodimer $[[CuH_{-1}L]_2]^{2+}$. In addition, peaks corresponding to the free ligand, $[CuL]^{2+}$, and $[CuH_{-2}L]$ species are also very significant, which reflects the variety of species found in the distribution diagram at this pH value (see Figure S8, Supporting Information). Smaller clusters for $[[CuH_{-2}L]_2+Na]^+$ (691.2) or with the general composition $[[CuH_{-2}L]_x+MM']^{2+}$, where M and M' can be either Na^+ or K^+, are also observed, for up to values of $x = 7$. From pH 7 to 12, only peaks derived from $[CuH_{-2}L]$ are detected. The base peak is the expected $[[CuH_{-2}L]+Na]^+$ species, and the dimer $[[CuH_{-2}L]_2+Na]^+$ only accounts for less than 20% of the intensity of the base peak. Again, as shown by the isotopic pattern, this peak also contains a contribution from the doubly charged cluster $[[CuH_{-2}L]_4+Na_2]^{2+}$. Very small peaks corresponding to higher order clusters $[[CuH_{-2}L]_x+Na_2]^{2+}$ are also detected.

For ligand **4c** at pH = 6.3, $[CuL]^{2+}$ species are the most important ones according to the distribution diagram, and the base peak in the ESI-MS at 408.1 corresponds to the $[[CuL]+AcO]^+$ species. The peak assigned to $[CuH_{-1}L]$ at 348.1 is also important (90%), and of minor importance are the peaks for $[[CuH_{-2}L]+K]^+$ at 386.1 and the dimer $[[CuH_{-1}L]_2+AcO]^+$ at 755.3. At pH = 7, $[CuL]$, $[CuH_{-1}L]$, and $[CuH_{-2}L]$ species coexist, but $[CuL]$ is very minor. Accordingly, the three most relevant peaks are those for $[CuH_{-1}L]^+$ at 348.1 (100%), $[[CuH_{-2}L]+Na]^+$ at 370.1 (80%), and $[[L]+Na]^+$ at 309.2 (70%). Small peaks for the complex clusters $[[CuH_{-2}L]_x+MM']^{2+}$ can be observed. At pH = 12, the MS is very similar to the one at pH = 7, but the peak assigned to $[[CuH_{-2}L]+Na]^+$ is the base peak, while the peak at 348.2 seems to correspond mainly to $[CuH_{-1}L]_2^{2+}$. In methanol, under basic conditions, the two more significant peaks appear at 386.1 for $[[CuH_{-2}L]+Na]^+$ and at 735.2 for $[[CuH_{-2}L]_2+Na]^+$.

In the case of the receptor with a spacer containing five methylene groups, **4d**, the predominant species at pH = 6.5

are $[CuL]^{2+}$ (ca. 60%) and $[[CuH_{-1}L]^+$ (ca. 20%). In good agreement with this, the base peak at this pH value appears at 422.1, corresponding to the monocation $[[CuL]+AcO]^+$ and the dication $[[CuL]+AcO]_2^{2+}$. The second, more important peak is observed for the $[CuH_{-1}L]^+$ species at 362.2 (58%) involving also $[[CuH_{-1}L]_2]^{2+}$ species. Rather interestingly, for this ligand, the ESI^+-MS presents small peaks that can be assigned to mononuclear Cu^{2+} complexes containing two ligand fragments. So, the MS contains peaks at 662.4 (17%) and 722.4 (<10%) that can be assigned, respectively, to the species $[Cu+L+H_{-1}L]^+$ and $[[CuL_2]+AcO]^+$. A cluster at 783.4 (<10%) containing two copper atoms, according to the isotopic pattern, can be associated with the $[[CuH_{-1}L]_2+AcO]^+$ species. Very similar peaks are observed at pH = 8, where $[CuH_{-1}L]^+$ largely predominates (ca. 85%), with a minor contribution from $[CuL]^{2+}$ (ca. 10%). At this pH, however, the peak at 362.2 contains a very important contribution from the dimeric cluster $[[CuH_{-1}L]_2]^{2+}$. It is worth mentioning that at pH = 12, essentially no peaks assignable to the expected $[CuH_{-2}L]$ species are detected, with the exception of the $[[CuH_{-2}L]+Na]^+$ peak at 384.1. Instead, the peaks associated with the free ligand are the most important, along with some smaller peaks than can be assigned to species derived from the $[CuH_{-1}L]^+$ complex. This seems to indicate either a much lower stability of the $[CuH_{-2}L]$ complexes for this ligand or, alternatively, the presence of complexes of a polymeric nature that cannot be transferred to the vapor phase without destroying their structure. In this case, the influence of the solvent appears to be very important, and in the case of the complexes formed in methanol, the corresponding peaks for $[[CuH_{-2}L]+K]^+$ (400.1, 100%) or for the corresponding dimer $[[CuH_{-2}L]_2+K]^+$ (763.3) are observed. This change in the nature of the complexes formed by the ligands with the larger spacers is confirmed by the fact that for the ligand **4e** no peaks corresponding to Cu^{2+} complexes could be detected either in water or in methanol.

Thus, although complex clusters containing several molecules of the corresponding bis-deprotonated copper complex are observed for ligands **4a**−**c** along with the peaks attributed to the molecular complexes, the absence of such molecular peaks for **4d**,**e** suggest that, in particular in water, polymeric complexes are predominant for the larger ligands. It must be also noted that, in general, the trend toward the formation of dimeric or oligomeric complexes seems to be larger for $[CuH_{-1}L]^+$ species in the case of ligands **4a**−**c** and in particular for the first one.

The structures of the Zn^{2+} species, at different pH values, were then examined by mass spectrometry. In this case, the experiment could not be carried out in water because of the slow precipitation of the corresponding species. Accordingly, all the mass spectra were obtained in methanol. The much lower stability constants for Zn^{2+} complexes were clearly reflected in the results obtained by ESI MS. Thus, by the use of the positive detection mode ($ESI-MS^+$), the species derived from $[ZnH_{-2}L]$ could not be observed under any conditions. This is reasonable since the observation of the peak involves protonation or interaction with an additional cation (i.e., Na^+ or K^+), which is enough to destroy the complex. Accordingly, only peaks derived from $[L]$ are observed at basic pH. At pH values closer to neutrality (pH = 8), $[ZnL]^{2+}$ species are observed. As shown in the distribution diagram, $[ZnL]^{2+}$ complex species are present in the pH window 5−9,
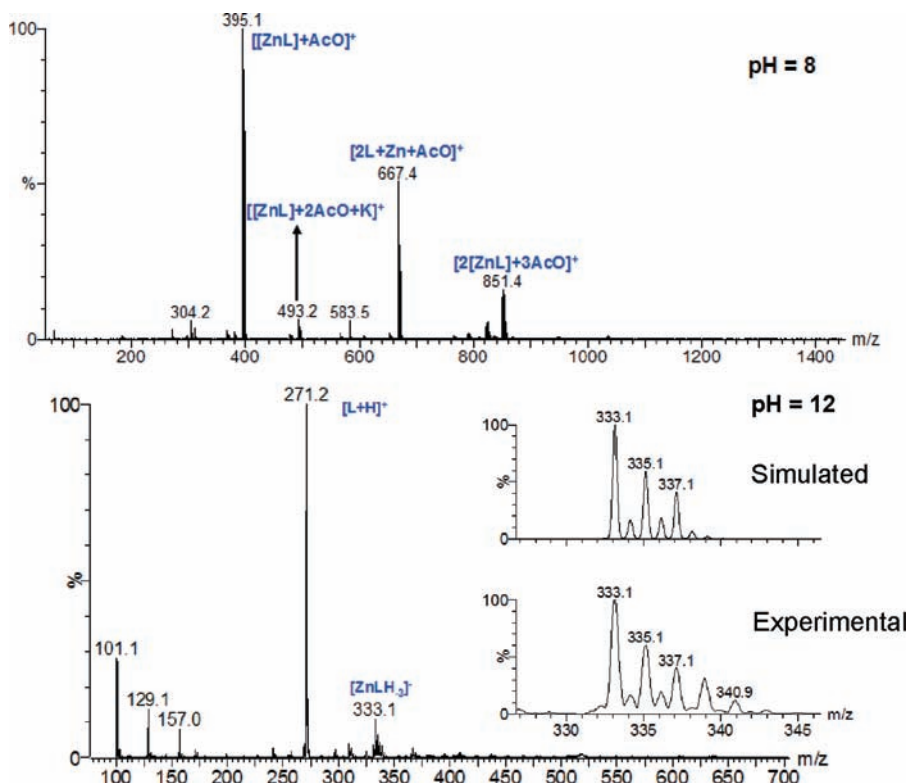
Figure 9. ESI-MS$^+$ spectra for Zn^{2+} and ligand **4b** at pH = 8 (top) and ESI-MS$^-$ at pH = 12 (bottom), both in methanol.

although those species are very minor. It must be noted that under those conditions (methanolic solutions at pH = 8), essentially the same spectra were obtained for compounds **4** independently of the aliphatic spacer. The most intense fragment is the one attributed to the monocation [[ZnL]+AcO]$^+$. The species [[ZnL$_2$]+AcO]$^+$ is also detected. A peak of lower intensity (10%) can be assigned to the species [[ZnL]+2AcO+Na]$^+$. Additional fragments, corresponding either to the free ligand (i.e., [L+K]$^+$ or [2L+K]$^+$) or to [ZnL]$^{2+}$ clusters are also detected. The situation is different for ESI-MS$^-$. In this case, ionization can take place by an additional deprotonation, and the neutral [ZnH$_{-2}$L] species is transformed in the monoanionic [ZnH$_{-3}$L]$^-$ species that can be detected. Thus, at pH = 12, the fragments observed for compounds **4** correspond to the monoanionic deprotonated ligand ([H$_{-1}$L]) and to the [ZnH$_{-3}$L]$^-$ species. The observed trends in ESI-MS are illustrated in Figure 9 for **4b**.

X-Ray Diffraction Studies. Crystals of good quality for X-ray diffraction studies were obtained for the corresponding Cu^{2+} complexes of ligands **4a** and **4b**, but at different pH values (7 and 12, respectively). The structures obtained nicely confirm the formation of complexes with very different environments for the copper atoms, in good agreement with the results obtained with the former techniques.

Crystal Structure of [Cu(H$_{-2}$4b)]·CH$_3$CH$_2$OH (5b). Crystals of **5b** were grown by evaporating solutions of Cu(AcO)$_2$·H$_2$O and **4b** at pH = 12 in ethanol. The crystal structure revealed the formation of a mononuclear neutral complex with a 1:1 ligand/metal stoichiometry. The structure of **5b** consists of two practically equivalent [CuH$_{-2}$L] neutral complex units and ethanol molecules coming from the crystallization solvent. In each unit, the copper atoms are coordinated with square-planar geometry to the two

primary amines and to the two deprotonated amide nitrogen groups (Figure 10).

As expected, the Cu−amide nitrogen distances (average 1.92 Å) are shorter than the Cu−amine ones (average 1.99 Å). The most important structural parameters for the structure are gathered in Table 6.

Although all the N−Cu−N angles are close to 90°, it can be noticed that the angle of the six-membered chelate ring involving the two deprotonated amide groups is broader than the angles of the five-membered chelate rings involving amide and primary amine nitrogens. This is a well-known feature in complexes having alternated five-membered and six-membered chelate rings and represents a strain-free conformation in which the metal−ligand interactions are maximized.[34] Finally, the angle involving the primary amines in both complexes is in between the previous ones (Table 6). The two isopropyl groups of each are oriented toward different sides of the coordination plane. It is interesting to remark that the different units and ethanol molecules are interconnected between them through a hydrogen bond network. Bifurcated hydrogen bonds are formed between the carbonyl oxygen atom O31 and secondary nitrogen atoms N1 and N11 of identical units (O31−N1, 2.79 Å; O31−N11, 3.03 Å); the other carbonyl oxygen atom of this unit (O91) connects with a nitrogen of a different unit (O91−N11A, 2.84 Å). Hydrogen bonds are also formed between the ethanol molecules and the carbonyl oxygen atom C31A of the second unit. Figure 11 depicts the hydrogen bond network formed.

Crystal Structure of [Cu$_2$(H$_{-1}$4a)$_2$](ClO$_4$)$_2$ (6a). Crystals of **6a** were grown by evaporating water solutions of

---

(34) Fawcett, T. G.; Rudich, S. M.; Toby, B. H.; Lalancette, R. A.; Potenza, J. A.; Scugar, H. J. *Inorg. Chem.* **1980**, *19*, 940–945.
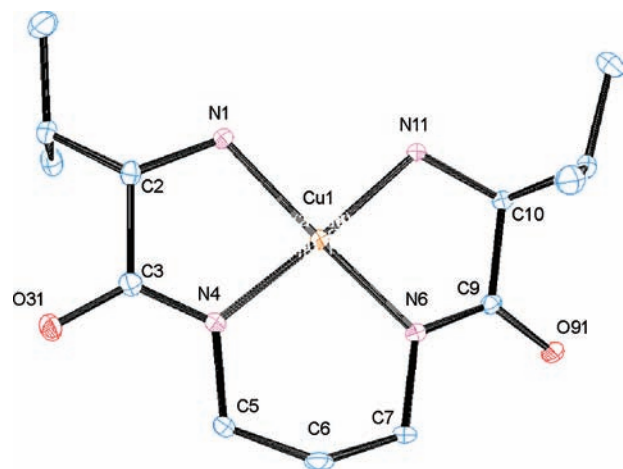
Figure 10. Molecular diagram for one out of the two [Cu(H$_{-2}$**4b**)] units present in **5b**. Ellipsoids at 50% probability level. Hydrogen atoms and solvent molecules have been omitted for clarity.
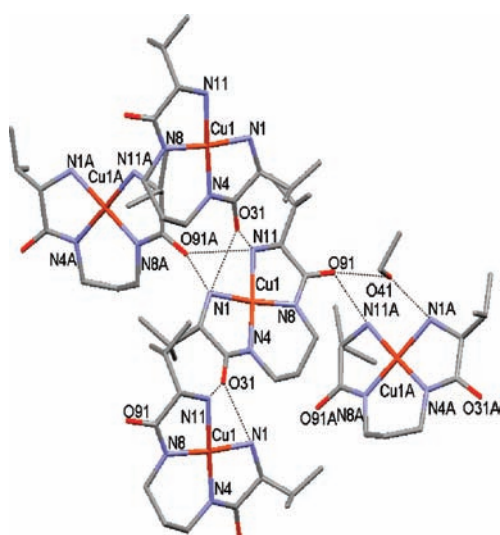

Figure 11. Schematic representation of the hydrogen bond network formed in compound [Cu(H$_{-2}$**4b**)]·CH$_3$CH$_2$OH (**5b**).

Table 6. Selected Bond Lengths (Å) and Angles (deg) for Compound **5b**[a]

Bond Distances			
Cu(1)−N(1)	1.982(2)	Cu(1A)−N(1A)	1.989(2)
Cu(1)−N(4)	1.924(2)	Cu(1A)−N(4A)	1.932(3)
Cu(1)−N(8)	1.916(2)	Cu(1A)−N(8A)	1.912(2)
Cu(1)−N(11)	1.991(2)	Cu(1A)−N(11A)	2.002(2)

Bond Angles			
N(1)−Cu(1)−N(4)	84.73(9)	N(1A)−Cu(1A)−N(4A)	82.37(11)
N(1)−Cu(1)−N(11)	92.67(9)	N(1A)−Cu(1A)−N(11A)	95.74(10)
N(4)−Cu(1)−N(8)	98.56(10)	N(4A)−Cu(1A)−N(8A)	97.71(10)
N(8)−Cu(1)−N(11)	83.91(10)	N(8A)−Cu(1A)−N(11A)	84.15(10)

[a] Data for the two slightly different [CuH$_{-2}$**4b**] complexes found in the asymmetric unit are presented.

Cu(ClO$_4$)$_2$·6H$_2$O and **4a** at an initial pH of 7. The crystal structure consists of [CuH$_{-1}$**L2**]$_2^{2+}$ cations and perchlorate counteranions. As shown in the distribution diagram included in Figure 4 (bottom), at this pH a species of [CuH$_{-1}$**L1**]$^+$ stoichiometry predominates in solution.
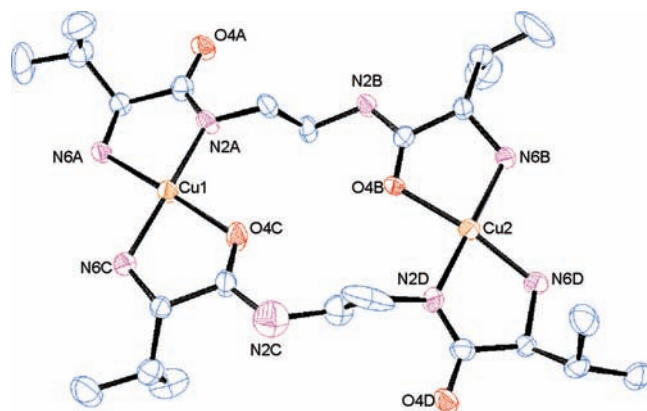

Figure 12. Molecular diagram of the [CuH$_{-1}$**4a**]$_2^{2+}$ subunit. Ellipsoids at the 50% probability level. Hydrogen atoms and solvent molecules have been omitted for clarity.

Table 7. Selected Bond Lengths (Å) and Angles (deg) for Compound **6a**

Bond Distances			
Cu(1)−N(2A)	1.922(8)	Cu(2)−N(2D)	1.917(10)
Cu(1)−O(4C)	1.979(8)	Cu(2)−O(4B)	2.039(7)
Cu(1)−N(6A)	1.983(8)	Cu(2)−N(6B)	1.989(8)
Cu(1)−N(6C)	1.998(9)	Cu(2)−N(6D)	1.999(10)
		Cu(2)−O(4D)	2.415(8)

Bond Angles			
N(2A)−Cu(1)−O(4C)	97.0(4)	O(4B)−Cu(2)−N(6B)	81.8(3)
N(2A)−Cu(1)−N(6A)	83.1(3)	N(6B)−Cu(2)−N(6D)	97.1(3)
O(4C)−Cu(1)−N(6C)	82.8(3)	N(6B)−Cu(2)−O(4D)	83.0(3)
N(6A)−Cu(1)−N(6C)	97.5(3)	N(6D)−Cu(2)−O(4D)	108.2(4)
N(2D)−Cu(2)−O(4B)	98.4(4)	N(2D)−Cu(2)−O(4D)	96.0(5)
N(2D)−Cu(2)−N(6D)	83.2(4)	O(4B)−Cu(2)−O(4D)	98.9(3)

According to ESI-MS experiments, a mixture of the monocationic species [CuH$_{-1}$**L1**]$^+$ and the dicationic dimer [CuH$_{-1}$**L1**]$_2^{2+}$ are responsible for the base peak. In general, [CuH$_{-1}$**L1**]$^+$ species tend to be detected as dimeric fragments.

The crystal structure of **6a** consists of a zigzag chain in which different [CuH$_{-1}$**L1**]$_2^{2+}$ dicationic dinuclear units are interconnected through coordinative bonds between Cu(2) and one oxygen atom of a deprotonated amide group of a neighbor unit (see Figures S12 and S13, Supporting Information).

Each [CuH$_{-1}$**L**]$_2^{2+}$ moiety contains two monodeprotonated ligands presenting an extended conformation and involving the coordination to two metal ions. The torsion angles in the chains that coordinate both metal sites are N2A−C1A−C1B−N2B, 173.7(8); C1A−C1B−N2B−C3B, 96.1(12); N2D−C1D−C1C−N2C, 174.6(10); and C1D−C1C−N2C−C3C, 128.5(19) (Figure 12).

In this basic unit, one copper atom, Cu(1), is coordinated in a square planar arrangement to two terminal primary amino groups of each ligand (N6A and N6C), to a nitrogen atom of a deprotonated amido group (N2A), and to the oxygen atom of a carbonyl group (O4C) of a neutral amide group of the other ligand (Figure 12).[35] As shown in Table 7,

(35) This type of chelating binding mode for amino acids is relatively common and, in particular, has been reported for copper(II) amino acid species: (a) Castellano, E. E.; Piro, O. E.; Casado, N. M. C.; Brondino, C. D.; Calvo, R. *J. Chem. Crystallogr.* **1998**, *28*, 61–68. (b) Tan, X. S.; Fujii, Y.; Sato, T.; Nakano, Y.; Yashiro, M. *Chem. Commun.* **1999**, 881–882.

the shortest Cu−N distance is the one with the deprotonated amino group (Cu(1)−N(2A), 1.922(8) Å). The bite angles are narrower than 90° when donor atoms of the same ligand are implicated and wider when donor atoms of the different ligands are implicated in the formation of the chelate rings (Table 7).

The second copper atom, Cu(2), displays a square-bipyramidal coordination geometry with significant axial distortion. The equatorial plane is defined by the nitrogen atom of a deprotonated amido group (N2D), which displays again the shortest Cu−N bond distance, two nitrogens of the terminal primary amino groups (N6B and N6D), and an oxygen atom (O4B) belonging to the carbonyl group of the nondeprotonated amine group.

The axial position is occupied by a carbonyl oxygen of a deprotonated amide belonging to a neighbor ligand molecule in the chain (Cu(2)−O(4D), 2.415(8) Å). Cu(2) is displaced 0.228 Å from the mean plane defined by the equatorial donor atoms toward the apical position. As previously commented upon, this axial coordination is the way in which the chain propagates, the angles between the mean coordination planes of the zigzag disposed dinuclear coordination $[[CuH_{-1}L]_2]^{2+}$ fragments being 79.6°. The chains are interconnected by bifurcated hydrogen bonds forming layers. The hydrogen bonds are established between the oxygen atom O4A of the deprotonated amide group and the primary amine nitrogens N6A and N6C (O4A−N6A, 2.919(13) Å; O4A−N6C, 3.051(11) Å; see the Supporting Information).

Conclusions

Pseudopeptidic ligands **4a**−**e** are able to form complexes of very different structures with metal ions such as Cu^{2+} and Zn^{2+}. A combination of pH-metric titrations, spectroscopic studies, and ESI-MS experiments has been carried out to analyze the complex formation. Two critical factors determining the final structure are the nature of the aliphatic spacer connecting the amino acid subunits and the pH value at which the complex is formed. Important differences can be found between Zn^{2+} and Cu^{2+} complexes. In the case of Zn^{2+}, the complexes, as expected, display much lower stability constants, but the most remarkable feature is that the length of the spacer seems to have a very minor influence on the nature of the complexes formed. While for Zn^{2+} the only complex species formed to a significant extent is the $[ZnH_{-2}L]$ species, for Cu^{2+} the situation is more complex. Bis-deprotonated $[CuH_{-2}L]$ species are the most stable complex species formed at basic pH values. The formation of those species is particularly important for the ligands with the shortest spacers (**4a**−**c**) for which deprotonation does not require very basic media. Monoprotonated $[CuH_{-1}L]^+$ complexes are always detected at lower pH values, although the participation of dimeric and oligomeric species with the general composition $[CuH_{-1}L]_x$ seems to be very important, in particular for the shorter ligand **4a** and for the larger ligands **4d**,**e**. In this regard, a clear, different behavior seems to be present when comparing ligands **4a**−**c** with **4d**,**e**. For the larger ligands, the formation of monomeric $[CuH_{-2}L]$ complexes is, apparently, not favored, and, instead, oligomeric/polymeric structures predominate. The crystals structures of the solid complexes $[Cu(H_{-2}L)]\cdot CH_3CH_2OH$ (**L** = **4b**) and $[Cu_2-(H_{-1}L)_2](ClO_4)_2$ (**L** = **4a**) confirm the former observations.

The first one confirms the monomeric nature and the formation of the expected deprotonated complex according to the general structure **5**, giving place to a square planar arrangement around the copper atom. The second structure obtained for **4a** at pH ≈ 7 reveals the presence of complex species with a general composition $[CuH_{-1}L]^+$ but involving dimeric $[CuH_{-1}L]_2^{2+}$ subunits with one square planar and one square pyramidal copper atom. Apical coordination of this second Cu with the carbonyl oxygen atom of another dimeric unit allows propagating the chain into a polymeric structure. In both cases, an extensive H-bonding network also involving the addition of anions or solvent molecules completes the interactions in the crystal.

Experimental Section

Electromotive Force Measurements. The potentiometric titrations were carried out at 298.1 K using 0.15 M $NaClO_4$ as a supporting electrolyte. The experimental procedure (buret, potentiometer, cell, stirrer, microcomputer, etc.) has been fully described elsewhere. The acquisition of the EMF data was performed with the computer program PASAT.[17] The reference electrode was a Ag/AgCl electrode in saturated KCl solution. The glass electrode was calibrated as a hydrogen-ion concentration probe by the titration of previously standardized amounts of HCl with CO_2-free NaOH solutions and the equivalent point determined by Gran's method,[36] which gives the standard potential, $E^{\circ\prime}$, and the ionic product of water [pK_w = 13.73(1)]. The computer program HYPERQUAD[16] was used to calculate the protonation and stability constants, and the HySS[17] program was used to obtain the distribution diagrams. The pH range investigated was 2.5−11.0, and the concentration of the metal ions and of the ligands ranged from 1×10^{-3} to 5×10^{-3} M with Cu^{2+}/**L** molar ratios varying from 2:1 to 1:2. The different titration curves for each system (at least two) were treated either as a single set or as separated curves without significant variations in the values of the stability constants. Finally, the sets of data were merged together and treated simultaneously to give the final stability constants.

Mass Spectrometry. Mass spectra were recorded on a hybrid QTOF I (quadrupole-hexapole-TOF) mass spectrometer with an orthogonal Z-spray-electrospray interface (Micromass, Manchester, U.K.) using either the electrospray positive mode (ES^+) or the electrospray negative mode (ES^-). The desolvation gas as well as nebulizing gas was nitrogen at a flow of 700 L/h and 20 L/h, respectively. The temperature of the source block was set to 120 °C and the desolvation temperature to 150 °C. A capillary voltage of 3.5 and 3.3 kV was used in the positive and negative scan modes, respectively. The cone voltage was typically set to 20 V to control the extent of fragmentation of the identified ions. Sample solutions were infused via syringe pump directly connected to the ESI source at a flow rate of 10 mL/min. The observed isotopic pattern of each intermediate perfectly matched the theoretical isotope pattern calculated from their elemental composition using the MassLynx 4.0 program.

NMR Measurements. The ^1H spectra were recorded on a Varian VNMR System 500 MHz spectrometer operating at 500 MHz. The solvent signal was used as a reference standard. Adjustments to the desired pH were made using drops of DCl or NaOD solutions. The pD was calculated from the measured pH values using the correlation pH = pD − 0.4.[37]

(36) (a) Gran, G. *Analyst* (*London*) **1952**, *77*, 661–671. (b) Rossotti, F. J.; Rossotti, H. *J. Chem. Educ.* **1965**, *42*, 375–378.

(37) (a) Glasoe, P. K.; Long, F. A. *J. Phys. Chem.* **1960**, *64*, 188–190. (b) Covington, A. K.; Paabo, M.; Robinson, R. A.; Bates, R. G. *Anal. Chem.* **1968**, *40*, 700–706.

Table 8. Crystallographic Data for $[Cu_2(H_{-1}4a)_2](ClO_4)_2$ (**6a**) and $[Cu(H_{-2}4b)] \cdot CH_3CH_2OH$ (**5b**)

	6a	5b
empirical formula	$C_{24}H_{50}Cl_2Cu_2N_8O_{12}$	$C_{15}H_{32}CuN_4O_3$
fw	840.70	379.99
cryst size, mm	$0.15 \times 0.1 \times 0.1$	$0.35 \times 0.28 \times 0.12$
cryst syst/s.g.	monoclinic	orthorhombic
space group	$P2_1$	$P2_12_12_1$
T K	293(2)	173(2)
λ(Mo Kα) (Å)	0.71073	0.71073
a, Å	13.4170(6)	10.191(2)
b, Å	9.8305(4)	10.771(2)
c, Å	14.0594(7)	35.070(5)
α, deg	90	90
β, deg	100.920(2)	90
γ, deg	90	90
V, Å^3	1820.80(14)	3849.5(12)
Z	2	8
d_{calc}, g/cm^3	1.533	1.311
abs coeff (mm^{-1})	1.381	1.153
F (000)	876	1624
reflecns collected	11791	46978
unique reflns	7064	8918
restraints	46	3
params	433	429
R1	0.0806	0.038
wR2	0.2805	0.082
GooF	1.04	1.03

Crystallographic Analysis. [CuH$_{-1}$4a]$_2$(ClO$_4$)$_2$ (6a). Crystals of **6a** suitable for X-ray analysis were obtained in 40% yield by slow evaporation of water solutions containing **4a** (0.017 g, 0.03 mmol) and Cu(ClO$_4$)$_2 \cdot$6H$_2$O (0.011 g, 0.03 mmol) adjusted to pH 7. Anal. Calcd for C$_{24}$H$_{50}$Cl$_2$Cu$_2$N$_8$O$_{12}$: C, 34.29; H, 5.99; N, 13.33. Found: C, 34.45; H, 5.75; N, 13.22.

Caution! Perchlorate salts of compounds containing organic ligands are potentially explosive and should be handled with care.

[CuH$_{-2}$4b]$\cdot$CH$_3$CH$_2$OH (5b). Yellow crystals of **5b** suitable for X-ray diffraction analysis were obtained by slow evaporation in an open vessel of ethanol solutions containing **4b** and Cu(OAc)$\cdot$H$_2$O in a 1:1 molar ratio (0.05 mol dm^{-3} concentrations) and at pH 12. Anal. Calcd for C$_{15}$H$_{32}$CuN$_4$O$_3$: C, 47.41; H, 8.49; N, 16.72. Found: C, 47.59; H, 8.46; N, 16.99.

Analysis of the single crystals of the complex from ligand **4a** was carried out with an Enraf-Nonius KAPPA CCD single-crystal diffractometer and that of the complex from ligand **4b** with a Siemens CCD three-circle diffractometer. In both cases, Mo Kα radiation ($\lambda = 0.71073$ Å) was used. The space groups were $P2_1$ and $P2_12_12_1$ for **6a** and **5b**, respectively. A total of 11 791 and 46 978 reflections were measured in the *hkl* ranges (-17, -12, -17) to (17, 9, 18) and (-13, -14, -46) to (13, 14, 46) between θ limits $1.5 < \theta < 27.4°$ and $2.0 < \theta < 28.4°$ for **6a** and **5b**, respectively. The structure was solved by the Patterson method using the program SHELXS-86,[38] running on a Pentium 100 computer. Isotropic least-squares refinement was performed by means of the program SHELXL-97.[39] The location of hydrogen atoms was inferred from neighboring sites. Crystal data, data collection parameters, and results of the analyses are listed in Table 8. During the final stages of the refinement, the positional parameters and the anisotropic thermal parameters of the non-hydrogen atoms were refined. The hydrogen atoms were refined with a common thermal parameter. Absolute structure was checked with Flack's parameter,[40] which resulted in 0.020(10) for **5b** and $-0.02(4)$ for **6a**. Molecular plots were produced with the ORTEP[41] and MERCURY programs.[42] See the Supporting Information for crystallographic data in electronic format.

Supporting Information Available: NMR titration for **4a**, distribution diagrams, UV−vis spectra, Job plots, and ESI$^+$-MS spectra. This material is available free of charge via the Internet at http://pubs.acs.org.

(38) Sheldrick, G. M.; Kruger, C.; Goddard, R. *Crystallographic Computing*; Clarendon Press: Oxford, England, 1985; p 175.

(39) Sheldrick, G. M *SHELXL-97*; Institut für Anorganische Chemie, University of Göttingen: Göttingen, Germany, 1997. (b) Sheldrick, G. M *Acta Crystallogr.* **2008**, *A64*, 112.

(40) Flack, H D *Acta Crystallogr.* **1983**, *A39*, 876.

(41) Johnson, C. K. *ORTEP*; Report ORNL-3794, Oak Ridge National Laboratory: Oak Ridge, TN, 1971.

(42) MERCURY 1.3 for Windows Me/2000/XP: (a) Taylor, R.; Macrae, C. F. *Acta Crystallogr.* **2001**, *B57*, 815–827. (b) Bruno, I. J.; Cole, J. C.; Edgington, P. R.; Kessler, M. K.; Macrae, C. F.; McCabe, J.; Pearson, J.; Taylor, R. *Acta Crystallogr.* **2002**, *B58*, 389–397.